A pH-oscillator Stretched in Space but Frozen in Time

Journal:	*The Journal of Physical Chemistry Letters*
Manuscript ID:	jz-2014-02711c.R1
Manuscript Type:	Letter
Date Submitted by the Author:	n/a
Complete List of Authors:	Hermans, Thomas; Université de Strasbourg, Institut de Science et d'Ingénierie Supramoléculaires Stewart, Peter; University of Glasgow , 2School of Mathematics and Statistics Grzybowski, Bartosz; Northwestern University, Chemical and Biological Engineering & Chemistry

A pH-Oscillator Stretched in Space but Frozen in Time

*Thomas M. Hermans[1†], Peter S. Stewart[2], Bartosz A. Grzybowski[1,]**

[1]Department of Chemical and Biological Engineering, Department of Chemistry, Northwestern University, 2145 Sheridan Rd., Evanston, IL 60208 (USA)

[2]School of Mathematics and Statistics, University of Glasgow, 15 University Gardens, Glasgow G12 8QW, UK

AUTHOR INFORMATION

Corresponding Author

*grzybor@northwestern.edu

Present Addresses

† Institut de Science et d'Ingénierie Supramoléculaires, 8 allée Gaspard Monge, Strasbourg (France).

ABSTRACT

Chemical oscillations are studied using a continuous-flow microfluidic system transforming the time domain of chemical oscillators into a spatial domain. This system allows one (i) to monitor the dynamics of chemical oscillators with the accuracy of vigorously stirred batch reactors, but with the ease and speed of CSTRs, and (ii) to rapidly screen the phase space of chemical oscillators in just one experiment vs. a traditional series of batch measurements.

TOC GRAPHICS

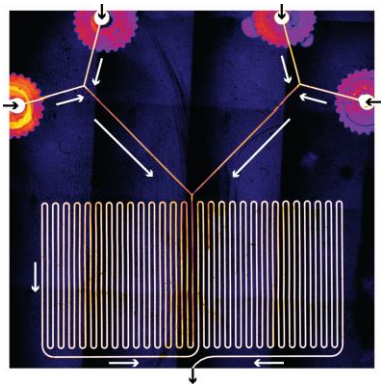

KEYWORDS Nonlinear chemical dynamics, chemical oscillator, complexity, microfluidics, reaction-diffusion.

Chemical oscillators play a key role in biological systems to regulate, for example, cellular signaling, cell locomotion, or rhythmicity of (cardiac) cells.[1] Since the pioneering works of Belousov and Zhabotinski in the 1960's,[2] oscillating reactions have also been realized in various ex-vivo chemical systems, and were recently interfaced with microscopic droplets[3–5], microparticles[6–8], liposomes[9], or nanoparticles[10,11], and also used to regulate vesicle-to-micelle transitions[12] or to create synthetic reaction networks[13]. Typically, chemical oscillators are studied in continuous stirred tank reactors (CSTRs),[14] whereby the reactants are pumped into a reactor of volume V at volumetric rate Q, while stirring at rate s. The CSTR allows one to sustain oscillations which, however, do not necessarily reflect system's inherent chemical dynamics and can be influenced by parameters s, Q and V. Alternatively, batch reactors can be used, which eliminates the influence of Q, but does not remove the dependence on the mixing quality, which is determined by s, V and the geometry of the reactor and of the stirring device.[15] These limitations raise a question of how one could rapidly and reliably measure the kinetics of a chemical oscillator without introducing artifacts due to the apparatus itself. The ideal reactor would have: 1) no spatial inhomogeneities in the concentration of any of the chemical species involved, 2) no distribution of residence times of various species in the reactor, and 3) no hysteresis or "memory" due to external control parameters such as Q, s, or V. These characteristics can be largely realized in microfluidic devices. Recently, enzymatic reactions have been studied in microfluidic systems that convert the reaction time domain to the space domain (i.e., length of the microfluidic channel), and in this way outperform traditional stopped-flow[16] and continuous-flow[17] kinetic measurements in terms of time resolution (< ms) and reagent consumption (< μL).[18,19] In another elegant study, Cronin and co-workers explored polyoxometalate assembly in both space and time domains to facilitate reproducible synthesis of

novel inorganic clusters.[20] Some oscillating and/or autocatalytic reactions[3,5,20,21] have also been explored using microfluidics. For instance, in the microfluidic Belousov-Zhabotinski systems, aqueous droplets were separated by hydrocarbons, allowing for communication and synchronization mediated by the diffusion of a bromine inhibitor; in such systems, uneven partitioning of chemical species into droplets has also been shown to cause various stochastic behaviors at low concentrations.[21,22] In the present work, we study chemical oscillation using one-phase microfluidic flows rather than microdroplets. As we show, this microflow chemistry approach allows us to (i) transform the time domain of chemical oscillators into a spatial domain, and (ii) measure the kinetics of chemical oscillators with the accuracy of vigorously stirred batch reactors, but with the ease and speed of CSTRs. The concentrations of the reactants can be changed rapidly and/or periodically without altering the total flow rate inside the device thus enabling our microfluidic platform to rapidly screen the phase space of chemical oscillators without introducing additional bifurcating parameters (e.g., Q, s) or the need to disperse the reaction mixture into small droplets.[3,18,19] The observation and conclusions of our work are supported by a mathematical model which shows in which domain of flow rate, diffusion coefficients, and reaction rates the device can be used.

We fabricated a continuous-flow microfluidic platform where the reactants are first mixed using passive micromixing geometries and thereafter flow through a long (~1 m) and narrow (200 μm) channel (Fig. 1). Our platform approaches the ideal apparatus outlined above, since the diffusive mixing time is fast compared to the reaction time (point 1 above), the chemical species react only with others of similar residence time (point 2), and the chemical dynamics does not show hysteresis (see below).

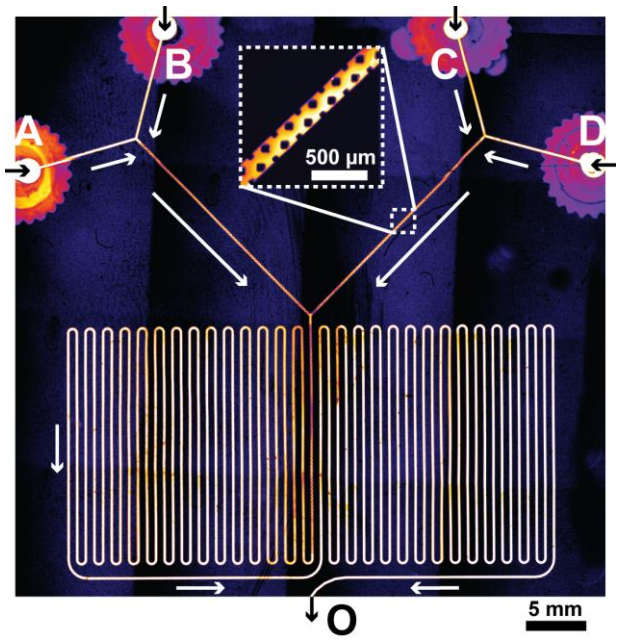

Figure 1. Confocal microscopy image of the microfluidic chip used to study pH oscillations. The system consists of four inlets (A, B, C, and D) and one outlet (O). Passive advective mixing is achieved by microposts inside the inlet channels (inset). The entire channel contains aqueous solution of rhodamine B (10 µM, white/yellow color) in order to visualize the chip by confocal microscopy. See also Fig. S1, S2.

Specifically, we used an all organic pH-oscillator in which base-catalyzed dehydration of methylene glycol increases the pH of the solution via OH^- production: $CH_2(OH)_2 + SO_3^{2-} \leftrightarrow CH_2(OH)SO_3^- + OH^-$. This so-called "clock" reaction was coupled to the base-catalyzed hydrolysis of gluconolactone producing H^+ (upon ring opening) and decreasing the solution's pH :[10,12,23] $C_6H_{10}O_6 + H_2O \leftrightarrow C_6H_9O_7^- + H^+$. This pH oscillator shows a single pH oscillation in batch, and sustained oscillations in a CSTR.[23] The chip contained four separate inlets labeled A, B, C, and D , and one outlet, O (Fig. 1, and Fig. S1, S2). Planar passive micromixing domains were used at three locations inside the channel to achieve good mixing at low Reynolds numbers

(*Re*).[24,25] The channels and mixing domains were made using a single step of SU-8 photolithography[26] followed by standard polydimethylsiloxane (PDMS) casting, curing, and bonding (see Experimental, part 1). First, flows A and B (termed AB after mixing) and, at the same time, C and D (resulting in flow CD) were mixed. Then, AB and CD flows were combined and mixed in the third micromixing domain (Fig. 1, vertical channel starting at the AB and CD junction and ending at the first 180° U-turn) resulting in a homogeneous solution (confirmed by fluorescence imaging) flowing over $L \approx 1$ m long serpentine-shaped channel to the outlet O.

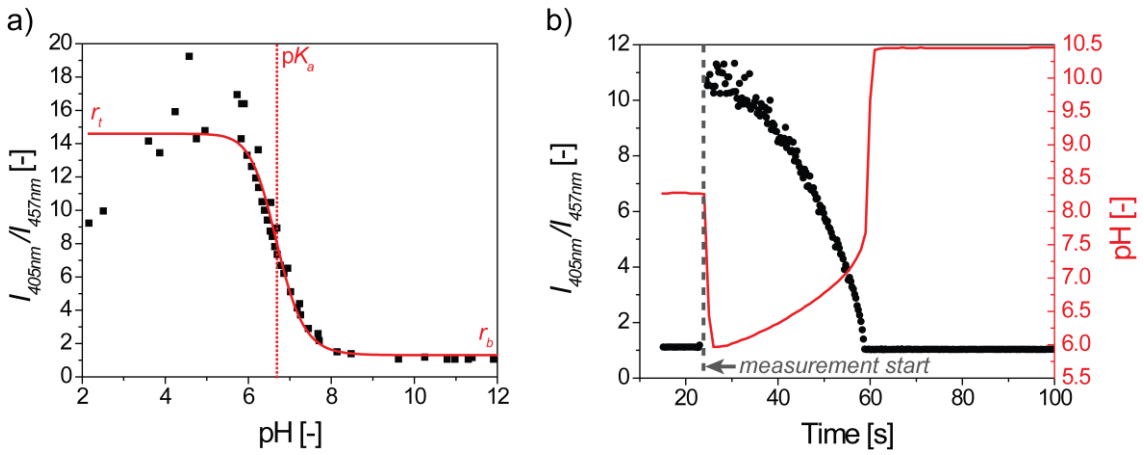

Figure 2. Spectroscopic measurement of pH. (a) HPTS (25 μM) in sulfite buffer was titrated using a concentrated aqueous solution of HCl (or KOH). Black squares are experimental data points; red line is the fit to eq. 1. Emission of HPTS at around 543 nm (acquired using a standard rhodamine filter cube) was measured first by excitation at 405 nm (resulting in emission intensity I405nm), followed by excitation at 457 nm (with emission intensity I_{457nm}). The ratio I_{405nm} / I_{457nm} was used to spectroscopically determine the pH in the range of 5.5–8.5. (b) Stirred batch experiment using "clock" conditions where the pH was measured using a pH meter (red line) and at the same time, the ratio I_{405nm} / I_{457nm} was recorded (black circles).

Next, we identified a method suitable for monitoring pH changes within our microfluidic system. In a stirred batch reactor, the "clock" methylene glycol–sulfite reaction results in a rapid increase from pH ~ 6 to pH ~10 within ~ 1 min (Fig. 2b, red line); this change can be recorded using a standard pH meter. However, a bulky pH meter cannot be fitted into the small microchannel – hence, we measured the pH spectroscopically using 8-hydroxypyrene-1,3,6-trisulfonic acid (HPTS), a fluorescent pH indicator whose absorption changes as a function of the degree of deprotonation (Fig. 2a). The pH was related to the ratio of HPTS emission intensities at 405 and 457 nm (see Experimental) via a Boltzmann sigmoidal function defined as:

$$I_{405nm} / I_{457nm} = r_t + (r_b - r_t) / \left(1 + e^{\frac{\mathrm{pH} - \mathrm{p}K_a}{dx}}\right) \qquad (1)$$

, where r_t is the highest ratio of I_{405nm} / I_{457nm}, r_b is the lowest ratio, dx the steepness of the curve, and the pK_a is for HPTS in the sulfite/metabisulfite buffer used here. By fitting eq. 1 to the experimental I_{405nm} / I_{457nm} values (black squares in Fig. 2a), we estimated the pK_a of HPTS at 6.7 ± 0.1, slightly lower than the value reported in phosphate buffer.[27] The range of pH that is accessible using this spectroscopic method with HPTS is 5.5–8.5, outside of which the ratio I_{405nm} / I_{457nm} does not change (e.g., pH = 12 will have the same I_{405nm} / I_{457nm} as pH = 9).

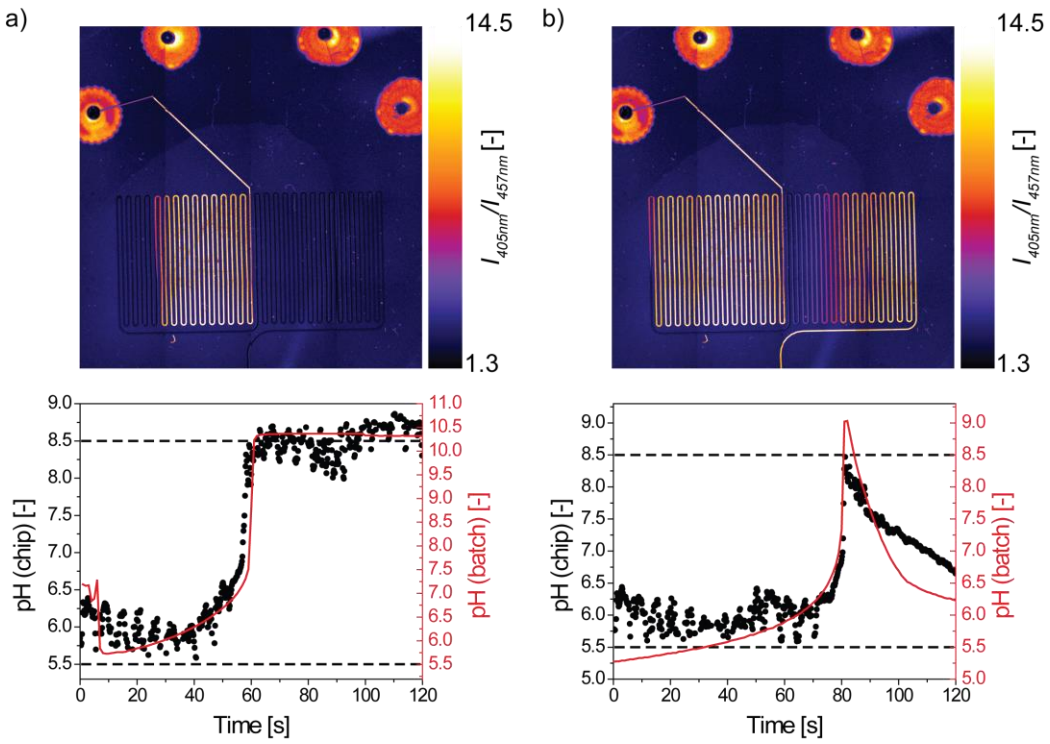

Figure 3. (a) pH of clock reaction mixture as measured using our microfluidic platform (black circles) and in a stirred batch reactor (red line). The experimental images above the graphs illustrate time-stationary profiles of pH: 5.5-7 for orange/yellow regions and 7-8.5 for purple/black regions. (b) Same as panel a, but for the oscillating reaction mixture. The dashed horizontal lines at pH = 5.5 and pH = 8.5 indicate, respectively, the lower and the upper limits of pH that can be measured using HPTS.

Next, we validated the spectroscopic measurement of pH in our microfluidic device. To this end, the "clock" conditions were again used and solutions of sulfite/metabisulfate buffer (inlet A and B containing **Sol1** and 100 μM of HPTS, see Experimental, part 3) and methylene glycol (inlets C and D with **Sol2**) were flowed at equal rates, resulting in a pH profile that changed along the length of the channel but did not change in time (Fig. 3a, top image). The position x along the channel (space domain) was converted to pseudo-time t' domain by dividing x by the

mean flow velocity <u>. This procedure gave a dependence (black markers in Fig. 3a) that agreed with the measurements of pH recorded in batch experiments (red line in Fig. 3a).

Upon addition of gluconolactone to the "clock" mixture discussed above, oscillatory conditions (*cf.* Experimental, part 4) were achieved such that 1) the onset of the rapid jump in pH was delayed, 2) the highest value of the pH was lowered, and 3) the pH decayed rapidly after the pH jump. The correspondence between the black markers and red line in Figure 3b indicates that results for the oscillating conditions in the batch reactor were, again, nearly identical to those measured in the microchannel. Altogether, the above considerations confirm that chemical kinetics underlying our reaction system is measured accurately using the microfluidic device in which the coordinate along the channel corresponds to reaction time.

It is instructive to consider theoretically the conditions under which such a transformation from time to space domain is valid. For the stirred batch reactor, the kinetics of our oscillating system can be described by a set of ordinary differential equations quantifying concentration changes of fourteen reactants, c_j (j = 1–14),

$$\frac{\partial c_j}{\partial t} = f_j(c_1,...,c_n) \qquad (2)$$

where f_j are functions governing the reactions and involve 14 rate constants k_i (i = 1–14; see reference [23] for all reactions and rate constants). In the microfluidic chip based on a channel of height 2h and length L, the concentration of each chemical species obeys an advection-diffusion-reaction partial differential equation (with constant diffusivity D_j)

$$\frac{\partial c_j}{\partial t} + u\frac{\partial c_j}{\partial x} + v\frac{\partial c_j}{\partial y} = D_j\left(\frac{\partial^2 c_j}{\partial x^2} + \frac{\partial^2 c_j}{\partial y^2}\right) + f_j(c_1,...,c_n) \qquad (3)$$

where x and y are the coordinates along and across the channel, and u and v are the corresponding liquid flow velocities, which follow from the Navier–Stokes equations[28]. Each chemical species is subject to no-flux boundary conditions through the channel walls.

In our experiment, the channel aspect ratio is $\varepsilon = h/L = 1 \times 10^{-4}$, which motivates an asymptotic expansion in the limit $\varepsilon << 1$. In this limit, the Navier–Stokes equations can be reduced to the familiar equations of lubrication[28], where the liquid velocity is a parallel Poiseuille flow with constant flow rate $Q = 2h\langle u \rangle$. The advection-diffusion equations can also be significantly reduced in this limit. In particular, by assuming $Q/D_j = \mathrm{O}(1)$ and $\varepsilon k_i / D_j = \mathrm{O}(1)$ it follows that the aspect ratio of the channel is small enough so that cross-stream diffusion is much faster than both the chemical reactions and the advection with the flow, which are in turn much faster than the streamwise diffusion. In this limit the cross-sectionally averaged concentration of each species, $\langle c_j \rangle$ satisfies the reduced advection-reaction equation,

$$\frac{\partial \langle c_j \rangle}{\partial t} + \langle u \rangle \frac{\partial \langle c_j \rangle}{\partial x} = f_j(\langle c_1 \rangle, ..., \langle c_n \rangle) \quad (4)$$

Then, the system can be represented in the advecting frame $z = x - \langle u \rangle t$, where each equation reduces to,

$$\frac{\partial \langle c_j \rangle}{\partial z} = f_j(\langle c_1 \rangle, ..., \langle c_n \rangle) \qquad (5)$$

identical to a batch reactor, when z is used as a time-equivalent coordinate (see SI, section 1 for derivation and additional comments in section 2). Overall, these mathematical considerations demonstrate that when the typical reaction timescale is slower than the timescale of diffusion across the microfluidic channel, but significantly faster than the timescale of diffusion along the channel, the governing equations for our microfluidic system are equivalent to those of a stirred batch reactor, consistent with experimental observations in Figure 3.

To validate our approach further, we performed the clock reaction at different flow rates Q (Fig. 4b). At higher Q values, the onset of the pH jump occurs further down in the channel (i.e., at larger values of L). However, all the curves overlap upon conversion to the time domain, by dividing the values of L by $\langle u \rangle$ (Fig. 4c). This overlap is nearly complete because the efficiency of the device's passive micromixing domains is insensitive with respect to Re.[24] In other words, the results we obtain are independent of the flow rate suggesting that the "time window" of the device could be adjusted (e.g., ~1–600 s is technically viable for pressure gradients that PDMS devices can withstand) to accommodate other chemical oscillators: for faster oscillations, a higher flow rate should be used, whereas for slower oscillations, the flow rate should be reduced. We also observe that upon increasing or decreasing Q and then returning to its initial value, the position of L corresponding to the onset of the pH jump returns reliably to the same location (i.e., the same L), showing there are no hysteresis effects in our microfluidic device, such as those commonly observed in the CSTR.[14,23,29]

Another useful characteristic of our microfluidic platform is that the reactant concentrations can be changed controllably in real time without changing the flow rate – this allows for rapid scanning of the oscillator's phase space. In an illustrative example, we supplied four different solutions into the device: sulfite/metabisulfite in inlets A and B with flowrates Q_A and Q_B (*cf.* Fig. 1), methylene glycol solution in inlet C (with Q_C), and methylene glycol/gluconolactone in inlet D (with Q_D). At t = 0, Q_A and Q_B were 2 μL min^{-1}, Q_C was 4, and Q_D was 0 μL min^{-1}.

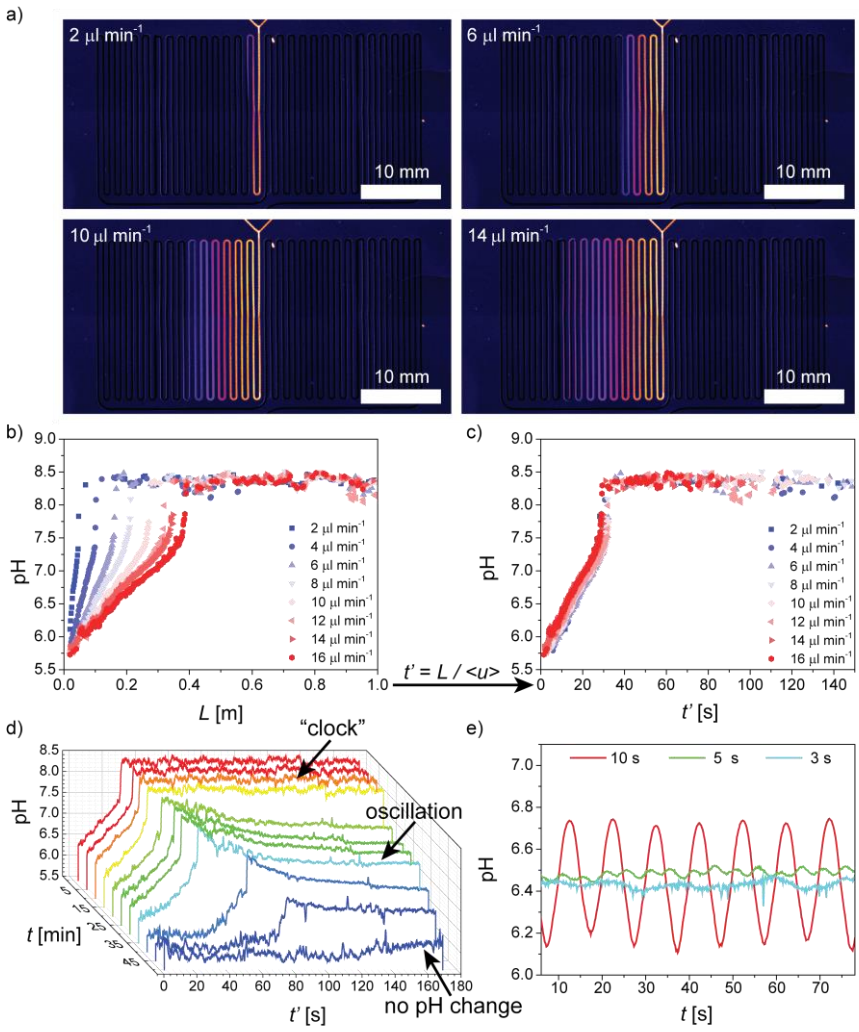

Figure 4. Spatial and temporal changes in pH measured inside the microchannel. (a) Confocal microscopy images showing a pH jump in the channel for the "clock" conditions at various flow rates Q. Inlet A: only metabisulfate (0.9507 g in 100 mL water), inlet B: sulfite/metabisulfite buffer with pH ~7 (0.9507 g metabisulfite & 0.5 g sulfite in 100 mL water), inlet C and D: **Sol2** (see Experimental, part 3). (b) the pH as a function of channel length L extracted from the images in panel a (and others, not shown). (c) The data of panel b is shown as a function of pseudo-time t', by dividing the values of L by the mean linear flow velocity $\langle u \rangle$. (d) Different behaviors observed while increasing the concentration of gluconolactone linearly in time (from 0 M at $t = 0$ to 0.056 M at $t = 60$ min.), while keeping the total flow rate equal to 8 μL min^{-1}. Inlets

A and B are identical to panels a,b,c. Inlet C: **Sol2** (see Experimental, part 4), inlet D: higher-concentration gluconolactone solution (1 g in 100 mL **Sol2**). (e) Profiles of pH recorded at a fixed location (L = 0.03 m) along the microfluidic channel while the inlet concentration of sulfite is changed periodically. The same conditions as in panels a,b,c were used.

This means that no gluconolactone was initially entering the device, and thus clock behavior was observed (Fig. 4d, red line). We then simultaneously (and linearly) decreased Q_C to 0 μL min^{-1} and increased Q_D to 4 μL min^{-1} over the course of 1h so that the combined flowrate Q_{CD} remained constant at 4 μL min^{-1}. Upon increasing the gluconolactone concentration (increasing t in Fig. 4d), the onset of the pH jump was increasingly delayed, the "clock" behavior gradually changed into an oscillation and finally, at the highest concentration, the pH changes were completely inhibited (dark blue t = 50 min line in Fig. 4d).

Lastly, we performed experiments in which the concentration of one of the reactants was changed periodically (sine function) instead of linearly as described above. Since the time to acquire a fluorescence image of the entire device is longer than the period of concentration change, for these experiments we measured the pH only at one fixed location (L = 0.03 m) along the channel using a fast resonant fluorescence detector (1500 frames per min., compared to 1 frame per min. for imaging the entire device). Specifically, we used clock conditions with a sulfite/metabisulfite buffer of pH 5.6 in inlet A, a sulfite/metabisulfite buffer of pH 7.0 in inlet B (titrated with more sulfite to reach the desired pH, see caption to Fig. 4) , and methylene glycol solution in inlets C and D (all four initially flowed at 2 μL min^{-1}). We then changed Q_A and Q_B between 0.1 and 3.9 μL min^{-1} sinusoidally with a period of 10, 5, or 3 s while keeping their combined flow rate Q_{AB} constant at 4 μL min^{-1} at all times (Fig. 4e). For the 10 s period (Fig. 4e, red line) the pH at L = 0.03 m closely followed the changes in sulfite concentration in flow AB.

For the 5 s period, the period could still be discerned, but the amplitude decreased significantly (Fig. 4e), because the time scale of streamwise diffusion and that of the imposed, sinusoidal oscillation period were commensurate. For even faster changes in the inlet concentration (3 s) streamwise diffusion equalized the sulfite concentration differences before reaching L = 0.03 m, and therefore only small aperiodic fluctuations in pH were observed (Fig. 4e). These experiments show that the inlet concentrations have to be changed slower than the axial dispersion time scale (> 10s). Importantly, these results are in line with the mathematical model discussed earlier, which indicates that as the flow rate decreases, the streamwise diffusion term becomes comparable to the advection along the channel (in particular, when $\langle u \rangle L/D_j$ = O(1) and k_i/D_j = O(1)).

In conclusion, we have demonstrated that microfluidic systems can be used to accurately and rapidly survey various concentration regimes under which nonlinear chemical phenomena such as oscillations can occur. The current approach is suitable for nonlinear reactions that are faster than 0.1 min^{-1}, and are detectable inside of microfluidic channels using spectroscopic methods such as UV-Vis or fluorescence. While the oscillator we studied here is a well-known one, we suggest that similar methodology can be used to screen other nonlinear systems whose phase space is not known a priori. Another possible extension is to use our platform for the discovery of batch pH oscillators,[30] which would be of great interest when coupled to pH-responsive materials for chemomechanical actuation.[31] Overall, we believe that microfluidics can provide a powerful for the discovery and characterization of nonlinear chemical systems.

EXPERIMENTAL SECTION

1. Microfluidic device fabrication / operation. Masters for microfluidic devices were fabricated by conventional photolithography in 100 μm layers of SU-8 50 photoresist (Microchem Corp.) These masters were then replicated into polydimethylsiloxane (PDMS, Dow Corning Sylgard 184) in a 10:1 base-to-crosslinker ratio. Holes for the fluid inlets/outlets were punched using a blunt needle, and the device was plasma-bonded onto a flat sheet of cured PDMS. Nanoport connectors (Upchurch/IDEX health & science) were embedded in a second layer of PDMS to allow tubing to be easily connected to the microfluidic device. Four syringe pumps (neMESYS, Cetoni GmbH) with independently controllable flow rates were used. The intensity ratio I405nm/I457nm was determined by using the segmented line, and plot profile tools in ImageJ 1.46r (http://rsbweb.nih.gov).

2. Imaging of microfluidic device. Confocal laser scanning microscopy was performed on a Nikon A1 system using a 1X (CFI Plan Achromat UW, Nikon) objective and image stitching (NIS Elements, Nikon) of typically 16 images (total frame time ~1 min). Ratiometric measurements with dual excitation at 405 nm and 457 nm were used to spectroscopically determine the pH inside the microchannel using 8-Hydroxypyrene-1,3,6-trisulfonic acid (Sigma-Aldrich). For the experiments in Fig. 4e the resonant scanner (Nikon; 25 frames per s) was used.

3. Clock conditions. The sulfite/metabisulfite buffer (**Sol1**) was prepared by dissolving 0.95069 g of sodium metabisulfite (Sigma-Aldrich) and 0.12609 g of sodium sulfite (Sigma-Aldrich) in 100 mL of ultrapure water, and degassed by purging with nitrogen. The solution was prepared fresh on a daily basis. The methylene glycol solution (**Sol2**) was prepared by diluting (9 mL in 591 mL of ultrapure water) a commercially available formaldehyde solution (~37% w/w, VWR) at least 24 h before use, and degassed by purging with nitrogen. **Sol2** could be used for several weeks. For batch experiments, 2 mL of **Sol1** and 2 mL of **Sol2** were added

simultaneously to a 50 mL falcon tube (VWR) and mixed vigorously (and continuously) using a vortex mixer (VWR). A pH meter (Mettler Toledo) was used to measure the pH as a function of time inside the tube. For clock experiments inside the microfluidic device, **Sol1** was pumped into inlet A and B, and **Sol2** into inlet C and D at 4 μL min^{-1} for each of the four inlets (unless otherwise specified).

4. Oscillation conditions. The gluconolactone solution (**Sol3**) was prepared by dissolving 0.23920 g of D-(+)-gluconic acid δ-lactone (Sigma-Aldrich) in 100 mL of **Sol2**, degassed using nitrogen and, because of degradation, used for no more than 45 min. In batch experiments, 2 mL of **Sol1** and 2 mL of **Sol3** were simultaneously added to a 50 mL falcon tube and mixed continuously on a vortex mixer, while measuring the pH with a pH meter. For oscillation experiments inside the microfluidic device, **Sol1** was pumped into inlet A and B, and **Sol3** into inlet C and D at 4 μL min^{-1} for each of the four inlets (unless otherwise specified).

ASSOCIATED CONTENT

Additional experimental information and a detailed derivation of the presented equations in described in the supporting information. This information is available free of charge via the Internet at http://pubs.acs.org.

AUTHOR INFORMATION

Corresponding Author

*Email: grzybor@northwestern.edu

ACKNOWLEDGMENT

This work was supported by the Non-equilibrium Energy Research Center which is an Energy Frontier Research Center funded by the U.S. Department of Energy, Office of Science, Office of Basic Energy Sciences under Award Number DE-SC0000989. T.M.H. was funded by the Human Frontier Science Program. The authors would like to thank Prof. Kyle J.M. Bishop for helpful suggestions.

REFERENCES

(1) Soh, S.; Byrska, M.; Kandere-Grzybowska, K.; Grzybowski, B. A. Reaction-Diffusion Systems in Intracellular Molecular Transport and Control. *Angew. Chem. Int. Ed.* **2010**, *49*, 4170–4198.
(2) Degn, H. Effect of Bromine Derivatives of Malonic Acid on the Oscillating Reaction of Malonic Acid, Cerium Ions and Bromate. *Nature* **1967**, *213*, 589–590.
(3) Toiya, M.; Vanag, V. K.; Epstein, I. R. Diffusively Coupled Chemical Oscillators in a Microfluidic Assembly. *Angew. Chem.* **2008**, *120*, 7867–7869.
(4) Delgado, J.; Li, N.; Leda, M.; González-Ochoa, H. O.; Fraden, S.; Epstein, I. R. Coupled Oscillations in a 1D Emulsion of Belousov–Zhabotinsky Droplets. *Soft Matter* **2011**, *7*, 3155–3167.
(5) Toiya, M.; González-Ochoa, H. O.; Vanag, V. K.; Fraden, S.; Epstein, I. R. Synchronization of Chemical Micro-Oscillators. *J. Phys. Chem. Lett.* **2010**, *1*, 1241–1246.
(6) Taylor, A. F.; Tinsley, M. R.; Wang, F.; Huang, Z.; Showalter, K. Dynamical Quorum Sensing and Synchronization in Large Populations of Chemical Oscillators. *Science* **2009**, *323*, 614–617.
(7) Tinsley, M. R.; Taylor, A. F.; Huang, Z.; Showalter, K. Emergence of Collective Behavior in Groups of Excitable Catalyst-Loaded Particles: Spatiotemporal Dynamical Quorum Sensing. *Phys. Rev. Lett.* **2009**, *102*, 158301.
(8) Taylor, A. F.; Tinsley, M. R.; Wang, F.; Showalter, K. Phase Clusters in Large Populations of Chemical Oscillators. *Angew. Chem.* **2011**, *123*, 10343–10346.
(9) Tomasi, R.; Noël, J.-M.; Zenati, A.; Ristori, S.; Rossi, F.; Cabuil, V.; Kanoufi, F.; Abou-Hassan, A. Chemical Communication between Liposomes Encapsulating a Chemical Oscillatory Reaction. *Chem. Sci.* **2014**, *5*, 1854–1859.
(10) Lagzi, I.; Kowalczyk, B.; Wang, D.; Grzybowski, B. A. Nanoparticle Oscillations and Fronts. *Angew. Chem. Int. Ed.* **2010**, *49*, 8616–8619.
(11) Nabika, H.; Oikawa, T.; Iwasaki, K.; Murakoshi, K.; Unoura, K. Dynamics of Gold Nanoparticle Assembly and Disassembly Induced by pH Oscillations. *J. Phys. Chem. C* **2012**, *116*, 6153–6158.
(12) Lagzi, I.; Wang, D.; Kowalczyk, B.; Grzybowski, B. A. Vesicle-to-Micelle Oscillations and Spatial Patterns. *Langmuir* **2010**, *26*, 13770–13772.
(13) Gerdts, C. J.; Sharoyan, D. E.; Ismagilov, R. F. A Synthetic Reaction Network: Chemical Amplification Using Nonequilibrium Autocatalytic Reactions Coupled in Time. *J. Am. Chem. Soc.* **2004**, *126*, 6327–6331.
(14) Epstein, I. R.; Pojman, J. A. *An Introduction to Nonlinear Chemical Dynamics: Oscillations, Waves, Patterns, and Chaos*; Oxford University Press, USA, 1998.
(15) Dutt, A. K.; Menzinger, M. Effect of Stirring and Temperature on a Belousov-Zhabotinskii-like Reaction in a Batch Reactor. *J. Phys. Chem.* **1992**, *96*, 8447–8449.
(16) Gibson, Q. H.; Milnes, L. Apparatus for Rapid and Sensitive Spectrophotometry. *Biochem. J.* **1964**, *91*, 161.
(17) Hartridge, H.; Roughton, F. J. W. A Method of Measuring the Velocity of Very Rapid Chemical Reactions. *Proc. R. Soc. Lond. Ser. Contain. Pap. Math. Phys. Character* **1923**, *104*, 376–394.
(18) Song, H.; Tice, J. D.; Ismagilov, R. F. A Microfluidic System for Controlling Reaction Networks in Time. *Angew. Chem. Int. Ed.* **2003**, *42*, 768–772.

(19) Song, H.; Ismagilov, R. F. Millisecond Kinetics on a Microfluidic Chip Using Nanoliters of Reagents. *J. Am. Chem. Soc.* **2003**, *125*, 14613–14619.
(20) De la Oliva, A. R.; Sans, V.; Miras, H. N.; Yan, J.; Zang, H.; Richmond, C. J.; Long, D.-L.; Cronin, L. Assembly of a Gigantic Polyoxometalate Cluster {W200Co8O660} in a Networked Reactor System. *Angew. Chem. Int. Ed.* **2012**, *51*, 12759–12762.
(21) Hasatani, K.; Leocmach, M.; Genot, A. J.; Estévez-Torres, A.; Fujii, T.; Rondelez, Y. High-Throughput and Long-Term Observation of Compartmentalized Biochemical Oscillators. *Chem. Commun.* **2013**, *49*, 8090–8092.
(22) Weitz, M.; Kim, J.; Kapsner, K.; Winfree, E.; Franco, E.; Simmel, F. C. Diversity in the Dynamical Behaviour of a Compartmentalized Programmable Biochemical Oscillator. *Nat. Chem.* **2014**, *6*, 295–302.
(23) Kovacs, K.; McIlwaine, R. E.; Scott, S. K.; Taylor, A. F. An Organic-Based pH Oscillator. *J. Phys. Chem. A* **2007**, *111*, 549–551.
(24) Bhagat, A. A. S.; Peterson, E. T. K.; Papautsky, I. A Passive Planar Micromixer with Obstructions for Mixing at Low Reynolds Numbers. *J. Micromechanics Microengineering* **2007**, *17*, 1017–1024.
(25) Hsieh, C. Y.; Yang, A. S. Mixing Enhancement of a Passive Micromixer by Applying Boundary Protrusion Structures. *Adv. Mater. Res.* **2009**, *74*, 77–80.
(26) Sokolov, A.; Apodaca, M. M.; Grzybowski, B. A.; Aranson, I. S. Swimming Bacteria Power Microscopic Gears. *Proc. Natl. Acad. Sci.* **2010**, *107*, 969–974.
(27) Wolfbeis, O. S.; Fürlinger, E.; Kroneis, H.; Marsoner, H. Fluorimetric Analysis. *Fresenius Z. Für Anal. Chem.* **1983**, *314*, 119–124.
(28) Acheson, D. J. *Elementary Fluid Dynamics*; Oxford University Press, 1990.
(29) Kovacs, K.; McIlwaine, R.; Gannon, K.; Taylor, A. F.; Scott, S. K. Complex Behavior in the Formaldehyde−Sulfite Reaction. *J. Phys. Chem. A* **2005**, *109*, 283–288.
(30) Csekõ, G.; Varga, D.; Horváth, A. K.; Nagypál, I. Simultaneous Investigation of the Landolt and Dushman Reactions. *J. Phys. Chem. A* **2008**, *112*, 5954–5959.
(31) Osada, Y. Conversion of Chemical into Mechanical Energy by Synthetic Polymers (chemomechanical Systems). In *Polymer Physics*; Advances in Polymer Science; Springer Berlin Heidelberg, 1987; pp. 1–46.

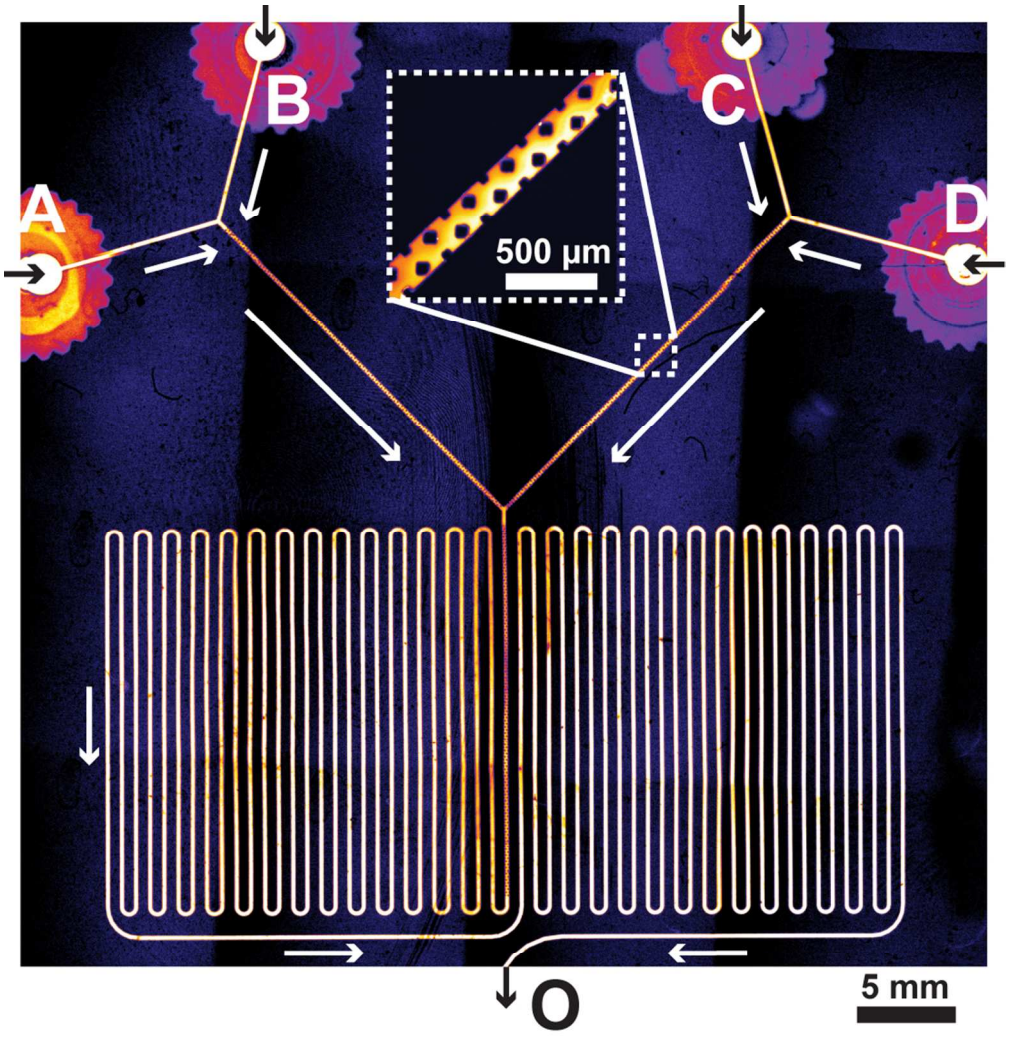

Figure 1. Confocal microscopy image of the microfluidic chip used to study pH oscillations. The system consists of four inlets (A, B, C, and D) and one outlet (O). Passive advective mixing is achieved by microposts inside the inlet channels (inset). The entire channel contains aqueous solution of rhodamine B (10 μM, white/yellow color) in order to visualize the chip by confocal microscopy. See also Fig. S1, S2.
186x195mm (150 x 150 DPI)

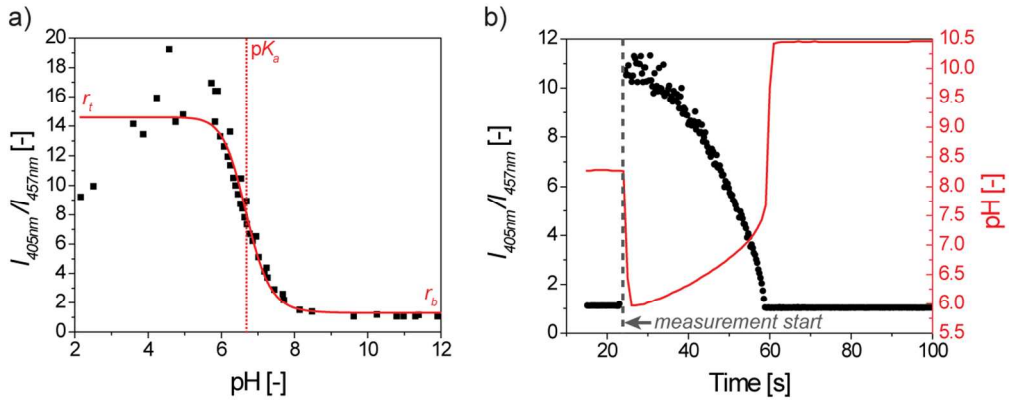

Figure 2. Spectroscopic measurement of pH. (a) HPTS (25 μM) in sulfite buffer was titrated using a concentrated aqueous solution of HCl (or KOH). Black squares are experimental data points; red line is the fit to eq. 1. Emission of HPTS at around 543 nm (acquired using a standard rhodamine filter cube) was measured first by excitation at 405 nm (resulting in emission intensity I405nm), followed by excitation at 457 nm (with emission intensity I457nm). The ratio I405nm / I457nm was used to spectroscopically determine the pH in the range of 5.5–8.5. (b) Stirred batch experiment using "clock" conditions where the pH was measured using a pH meter (red line) and at the same time, the ratio I405nm / I457nm was recorded (black circles).
219x87mm (150 x 150 DPI)

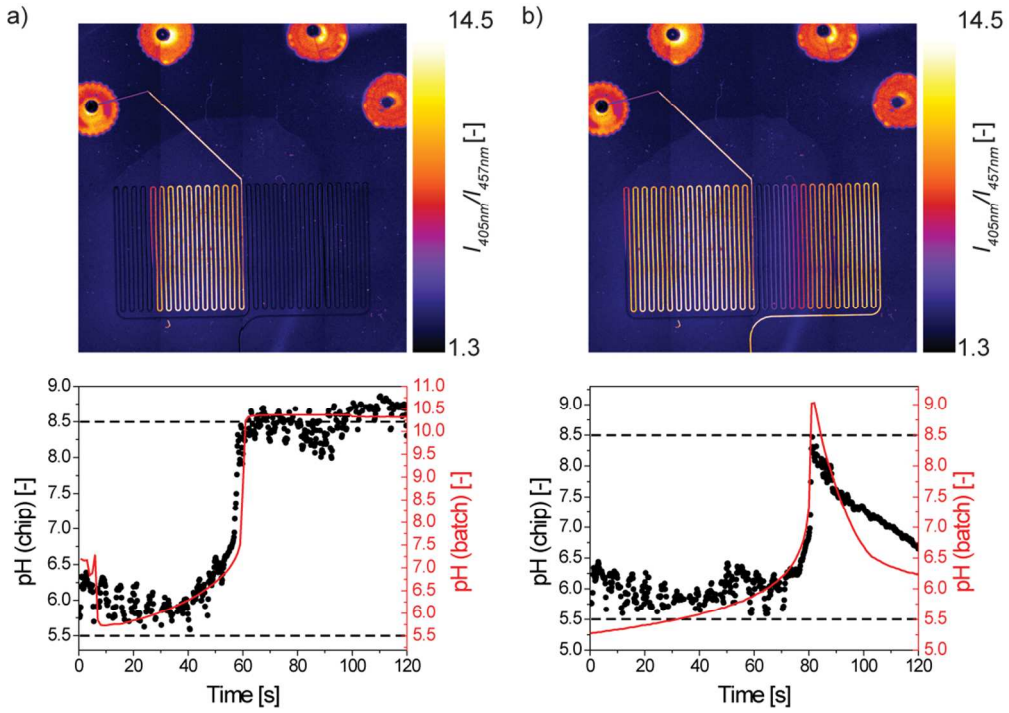

Figure 3. (a) pH of clock reaction mixture as measured using our microfluidic platform (black circles) and in a stirred batch reactor (red line). The experimental images above the graphs illustrate time-stationary profiles of pH: 5.5-7 for orange/yellow regions and 7-8.5 for purple/black regions. (b) Same as panel a, but for the oscillating reaction mixture. The dashed horizontal lines at pH = 5.5 and pH = 8.5 indicate, respectively, the lower and the upper limits of pH that can be measured using HPTS.
195x138mm (150 x 150 DPI)

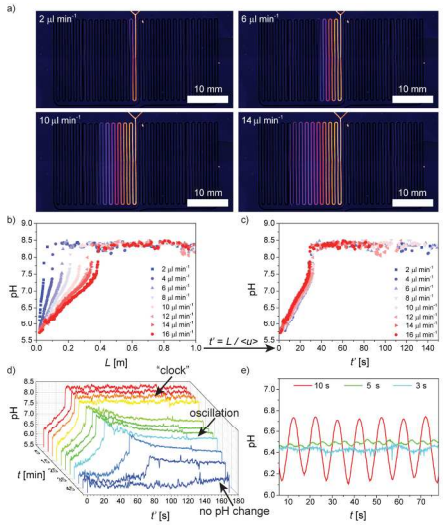

Figure 4. Spatial and temporal changes in pH measured inside the microchannel. (a) Confocal microscopy images showing a pH jump in the channel for the "clock" conditions at various flow rates Q. Inlet A: only metabisulfate (0.9507 g in 100 mL water), inlet B: sulfite/metabisulfite buffer with pH ~7 (0.9507 g metabisulfite & 0.5 g sulfite in 100 mL water), inlet C and D: Sol2 (see Experimental, part 3). (b) the pH as a function of channel length L extracted from the images in panel a (and others, not shown). (c) The data of panel b is shown as a function of pseudo-time t', by dividing the values of L by the mean linear flow velocity . (d) Different behaviors observed while increasing the concentration of gluconolactone linearly in time (from 0 M at t = 0 to 0.056 M at t = 60 min.), while keeping the total flow rate equal to 8 µL min-1. Inlets A and B are identical to panels a,b,c. Inlet C: Sol2 (see Experimental, part 4), inlet D: higher-concentration gluconolactone solution (1 g in 100 mL Sol2). (e) Profiles of pH recorded at a fixed location (L = 0.03 m) along the microfluidic channel while the inlet concentration of sulfite is changed periodically. The same conditions as in panels a,b,c were used.
438x231mm (150 x 150 DPI)

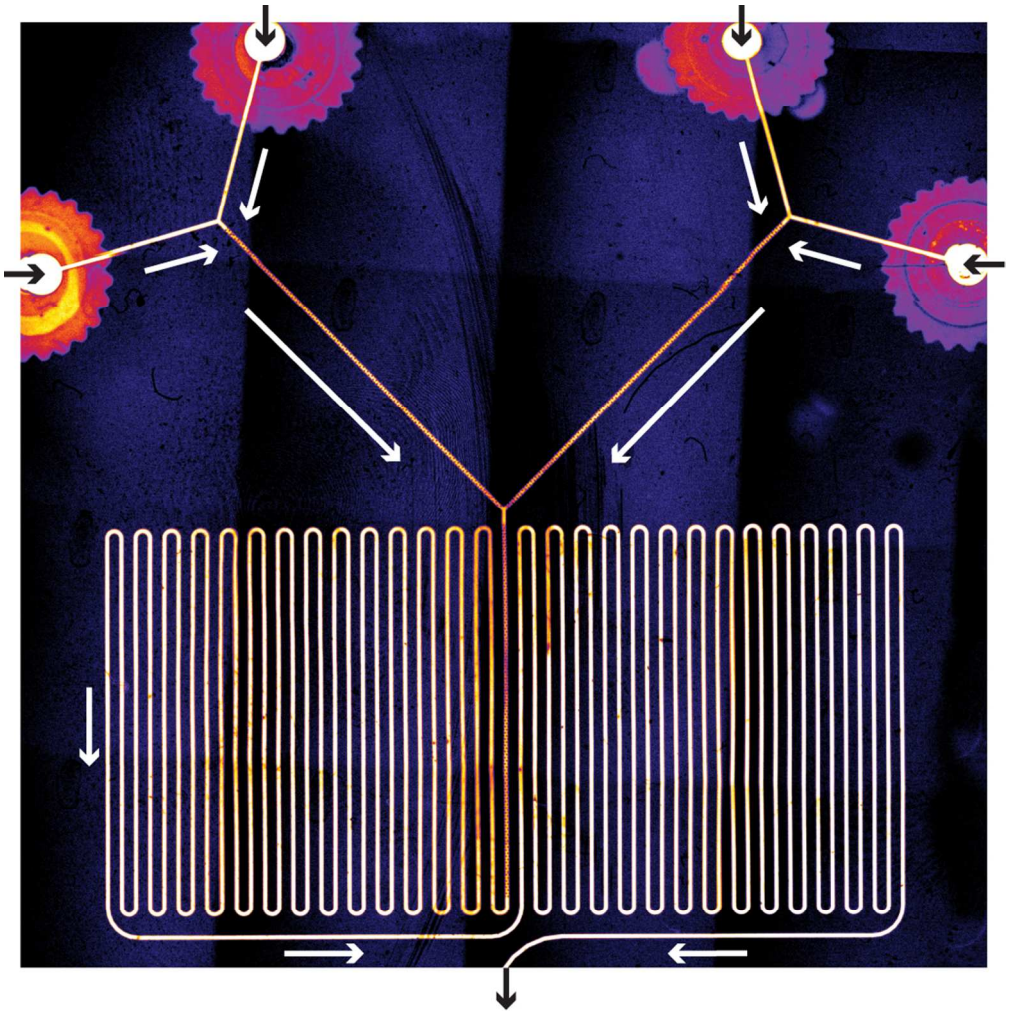

Table of contents graphic (TOC)
186x187mm (150 x 150 DPI)